

# Hierarchical TiN-Supported TsFDH Nanobiocatalyst for CO<sub>2</sub> Reduction to Formate

Federica Arena<sup>+</sup>,<sup>[a, b]</sup> Giorgio Giuffredi<sup>+</sup>,<sup>[a, b]</sup> Andrea Perego<sup>#</sup>,<sup>[a]</sup> Stefano Donini,<sup>[a]</sup> Hilmar Guzmán,<sup>[c]</sup> Simelys Hernández,<sup>[c]</sup> Eduardo Stancanelli,<sup>[d]</sup> Cesare Cosentino,<sup>[d]</sup> Emilio Parisini,<sup>[a]</sup> and Fabio Di Fonzo<sup>\*[a]</sup>

The electrochemical reduction of CO<sub>2</sub> to value-added products like formate represents a promising technology for the valorization of carbon dioxide. We propose a proof-of-concept bioelectrochemical system (BES) for the reduction of CO<sub>2</sub> to formate. For the first time, our device employs a nanostructured titanium nitride (TiN) support for the immobilization of a formate dehydrogenase (FDH) enzyme. The hierarchical TiN nanostructured support exhibits high surface area and wide pore size distribution, achieving high catalytic loading, and is characterized by higher conductivity than other oxide-based supports employed for FDHs immobilization. We select the oxygen-tolerant FDH from *Thiobacillus sp. KNK65MA* (TsFDH) as

enzymatic catalyst, which selectively reduces CO<sub>2</sub> to formate. We identify an optimal TiN morphology for the enzyme immobilisation through enzymatic assay, reaching a catalyst loading of 59 μg cm<sup>-2</sup> of specifically-adsorbed TsFDH and achieving a complete saturation of the anchoring sites available on the surface. We evaluate the electrochemical CO<sub>2</sub> reduction performance of the TiN/TsFDH system, achieving a remarkable HCOO<sup>-</sup> Faradaic efficiency up to 76%, a maximum formate yield of 44.1 μmol mg<sup>-1</sup> FDH h<sup>-1</sup> and high stability. Our results show the technological feasibility of BES devices employing novel, nanostructured TiN-based supports, representing an important step in the optimization of these devices.

## 1. Introduction

Electrochemical CO<sub>2</sub> reduction (CO<sub>2</sub>R) represents an appealing technology for the implementation of the carbon capture and utilization (CCU) strategy, since it allows CO<sub>2</sub> to be used as carbon source for the synthesis of carbon-neutral energy vectors, fuels and chemical feedstock. Nowadays, the state-of-art catalysts for this application are transition metals,<sup>[1–3]</sup> thanks to their high CO<sub>2</sub> conversion efficiency in terms of selectivity and product yield. Despite their remarkable efficiency, the energy efficiency of transition metal and their product specificity can be markedly improved.<sup>[3,4]</sup> Copper, the most employed

transition metal CO<sub>2</sub>R catalyst, evolves a mixture of products ranging from CO to CH<sub>4</sub> to more complex compounds like C<sub>2</sub>H<sub>4</sub>, C<sub>2</sub>H<sub>6</sub>, HCOO<sup>-</sup>,<sup>[5]</sup> with a selectivity depending on different parameters like catalyst morphology, crystalline structure, applied overpotential and surface coverage of intermediate species.<sup>[6,7]</sup> Sn and Pd, the state-of-art electrocatalysts for HCOO<sup>-</sup> production,<sup>[8,9]</sup> exhibit unsatisfactory energy efficiency when their morphology and composition are not finely tuned to the nanoscale.<sup>[10,11]</sup> Ag, which according to DFT calculations should reduce CO<sub>2</sub> selectively to CO,<sup>[12,13]</sup> evolves up to 6 different products.<sup>[14]</sup> The low product specificity is related to a complex reaction mechanism, with different pathways for different products according to catalyst-specific features as its surface composition,<sup>[15]</sup> adsorbates surface coverage<sup>[16]</sup> or morphological features.<sup>[17]</sup> This factor represents a drawback for the *a priori* design of a catalyst tailored to the synthesis of a specific product and is a significant challenge to be overcome for this technology.

Recently, the incorporation of biological organisms in inorganic electrocatalytic systems has created great opportunities for CO<sub>2</sub> reduction at limited overpotential,<sup>[18]</sup> with the development of two families of bioelectrochemical systems (BES): “microbial electrosynthesis” systems (MES)<sup>[19,20]</sup> and “enzymatic electrosynthesis” systems (EES).<sup>[21,22]</sup> MES exploits microbial metabolic pathways for CO<sub>2</sub> reduction, but is still economically uncompetitive because of the slow microbial reaction kinetics and the production of complex mixture of products, requiring further downstream processing. EES instead exploits enzymes to catalyze reactions with high conversion efficiency, high activity under controlled experimental conditions and higher selectivity towards both specific substrates and products than transition metal catalysts.<sup>[23,24]</sup> The substrate-specific prop-

[a] F. Arena,<sup>+</sup> Dr. G. Giuffredi,<sup>+</sup> Dr. A. Perego,<sup>#</sup> Dr. S. Donini, Dr. E. Parisini, Dr. F. Di Fonzo  
Center for Nano Science and Technology – Istituto Italiano di Tecnologia (IIT@Polimi)  
Via Pascoli 70/3, 20063 Milano, Italy  
E-mail: fabio.difonzo@iit.it


[b] F. Arena,<sup>+</sup> Dr. G. Giuffredi<sup>+</sup>  
Politecnico di Milano – Department of Energy  
Via Lambruschini 4, Milano, Italy


[c] H. Guzmán, S. Hernández  
Politecnico di Torino – Department of Applied Science and Technology  
Corso Duca degli Abruzzi 24, Torino, Italy

[d] E. Stancanelli, C. Cosentino  
Ronconi Institute for Chemical and Biochemical Research  
Via Colombo 81, Milano, Italy

[<sup>+</sup>] These authors contributed equally to the work.

[<sup>#</sup>] Present affiliation: National Fuel Cell Research Center, University of California Irvine, Irvine, CA 92617, USA

 Supporting information for this article is available on the WWW under <https://doi.org/10.1002/celec.202100480>

 © 2021 The Authors. ChemElectroChem published by Wiley-VCH GmbH. This is an open access article under the terms of the Creative Commons Attribution License, which permits use, distribution and reproduction in any medium, provided the original work is properly cited.

erty of enzymes allows the conversion of the CO<sub>2</sub> substrate with a theoretical 100% selectivity towards a specific product through a different pathway than transition metals, with lower energy barriers,<sup>[25]</sup> marginal overpotentials to reach satisfactory product yield,<sup>[26,27]</sup> and without the limiting energy scaling relations.<sup>[28]</sup> Taking inspiration from the three-enzyme catalytic cascade,<sup>[29,30]</sup> where CO<sub>2</sub> is sequentially converted into formate, formaldehyde and methanol, formate dehydrogenase (FDH) (EC 1.17.1.9) enzymes showed promise for the reversible and selective reduction of CO<sub>2</sub> to formate (HCOO<sup>-</sup>). FDHs from anaerobic bacteria are particularly appealing due to the high CO<sub>2</sub>R activity, arising from their active site which contains a metallic center (e.g. Mo or W) with fast turn-over frequency, with a calculated value of  $K_{\text{cat}} = 262 \text{ s}^{-1}$ .<sup>[31]</sup> Nevertheless, the metallic active site is oxygen-labile,<sup>[31–33]</sup> undergoing rapid deactivation during operation in atmosphere, which makes their industrial application unfeasible. Consequently, immobilization of the enzymatic component on an inorganic, nano-engineered support has proven to be efficient in improving the overall catalytic activity<sup>[34]</sup> and long-term stability of the FDH<sup>[35,36]</sup> with respect to its free form.<sup>[37]</sup> This strategy has found successful application in many BES systems employing oxygen-labile FDHs for electrocatalytic CO<sub>2</sub> reduction to formate, where the immobilization of the enzymatic catalyst on complex, nanostructured supports like mesoporous TiO<sub>2</sub> films,<sup>[38]</sup> inverse-opal TiO<sub>2</sub> architectures,<sup>[39]</sup> porous 3D networks based on polyaniline (PANI) hydrogel<sup>[40]</sup> or carbon cloth<sup>[41]</sup> allowed to optimize the enzyme loading and drastically enhance the catalytic activity and the formate yield. Despite the performance improvement granted by the support, the deactivation of the enzyme in atmosphere remains a critical drawback.

On the other hand, FDHs from aerobic bacteria or yeast, e.g. *C. boidinii* (CbFDH) are oxygen-tolerant and have longer stability than anaerobic FDHs; therefore, they have been widely studied for the CO<sub>2</sub> reduction to formate in BES systems.<sup>[42–44]</sup> Despite the longer stability, oxygen-tolerant FDHs have lower CO<sub>2</sub> reducing activity than anaerobic FDHs and require a NADH/NAD<sup>+</sup> cofactor to catalyze the CO<sub>2</sub>/HCOO<sup>-</sup> interconversion.<sup>[45]</sup> In these systems, the interaction between inorganic scaffold and enzyme has not been optimized, because the support is mainly exploited for the *in-situ* regeneration of the NADH/NAD<sup>+</sup> cofactor by an appropriate electron donor deposited on the electrode (usually, electrodeposited polymerized neutral red).<sup>[42–44]</sup> The most employed supports in these BES systems are based on carbon, e.g. graphite disks,<sup>[42]</sup> rods<sup>[43,46]</sup> or powder,<sup>[44]</sup> but their structure is not optimized for enzyme immobilization, since their morphology is flat and not nano-engineered. The flat nature of the support, along with the concurrent cofactor regeneration, drastically limits the maximum catalytic activity of the BES. Firstly, the conversion of the NADH/NAD<sup>+</sup> cofactor at cathodic potentials limits the maximum selectivity of the system towards formate. Additionally, because of the large size of the enzyme,<sup>[23]</sup> the catalytic turnover number per unit projected area is very low (despite the high catalytic activity of the single molecule). Moreover, when immobilization is performed by drop-casting the enzyme, a limited efficiency is achieved, with the enzyme not specifically adsorbed on the anchoring sites or

with the possible formation of aggregates with negligible activity arising from a misfolding of the proteins. In fact, the misfolding exposes the hydrophobic enzyme sites, which bind one with another, making the aggregate catalytically inactive.

This work demonstrates how a carefully nano-engineered support, namely a hierarchical titanium nitride (TiN) nanostructured electrode (HTNE), can enhance the overall productivity of oxygen-stable FDHs retaining their stability in aerobic conditions. The HTNE is synthesized by pulsed laser deposition (PLD), a physical vapor deposition technique that allows for fine-tuning the nano and meso scale morphology of the TiN nanostructures comprising the electrode, controlling surface area and pore structure. This is key to optimize the binding of the enzyme and to retain its activity. TiN is chosen as a support material thanks to its remarkable stability<sup>[47]</sup> in the electrochemical environment and high electrical conductivity.<sup>[48–53]</sup> Additionally, enzyme coupling is favored on TiN thanks to the transfer of s-valency and d-valency electrons of the Ti atoms to the 2p-states of N atoms,<sup>[52]</sup> therefore it is a promising material for enzyme immobilization. This nanostructured support is here coupled with an oxygen tolerant FDH from *Thiobacillus sp. KNK65MA* (TsFDH), chosen because of its higher CO<sub>2</sub> reducing activity (turnover number  $K_{\text{cat}} = 0.318 \text{ s}^{-1}$ ) than the commercially available CbFDH ( $K_{\text{cat}} = 0.015 \text{ s}^{-1}$ ).<sup>[54]</sup> Thanks to the optimized immobilization of the enzyme on the nanostructured support and to the TsFDH reducing activity, a remarkable CO<sub>2</sub>R performance is achieved, with a formate FE up to 76% and a high gravimetric product yield up to  $44.1 \mu\text{mol mg}_{\text{enzyme}}^{-1} \text{ h}^{-1}$ . These results are a promising step towards the implementation of efficient and stable BES systems based on oxygen-tolerant FDHs, with a particular focus on the formate yield. Noteworthy, these figures are comparable to what achieved by many oxygen-labile FDHs-based BES. Therefore, our proof-of-concept BES paves the way for a new and efficient class of hybrid electrocatalytic systems that couple oxygen-stable FDH enzymes with nano-engineered and optimized nanostructured highly conductive supports.

## 2. Results and Discussion

### 2.1. Characterization of Recombinant TsFDH

The FDH enzyme from *Thiobacillus sp. strain KNK65MA* (TsFDH) is chosen as catalyst for the reduction of CO<sub>2</sub> to HCOO<sup>-</sup>. In previous literature works,<sup>[54]</sup> TsFDH has been reported as the NAD-dependent enzyme with the highest CO<sub>2</sub> reduction activity, with a  $K_{\text{cat}}$  of  $0.318 \text{ s}^{-1}$ . As a comparison, the other NAD-dependent FDH from *Candida boidinii* (CbFDH) exhibits a CO<sub>2</sub> reduction activity that is roughly 20 times smaller, with a  $K_{\text{cat}}$  of  $0.015 \text{ s}^{-1}$ .<sup>[54]</sup>

The expression and purification of the recombinant TsFDH resulted in a pure (Figure SI 1) and active enzyme with a yield of 12.5 mg of protein per liter of bacterial culture (Table SI 1). The shelf-life stability of the enzyme, assessed by enzymatic assay described in Section 2.4 and reported in Figure SI 3, revealed a good activity over a broad period of time. Indeed,

the enzyme retained more than 75% of its initial activity after 24 h, and still a 20% of residual activity after 14 days. Stability retention over prolonged periods is crucial for maintaining a good catalytic activity of the FDH enzyme and thus for obtaining a stable bioelectrochemical electrode during CO<sub>2</sub> reduction. This result provides a promising starting point for the realization of a stable bioelectrochemical electrode with TsFDH immobilized on a TiN nanostructured surface. Starting from a remarkable shelf-life stability of the sole enzymatic component, we expect an even higher stability after the immobilization of the TsFDH on the TiN support. Indeed, it has been demonstrated that enzyme immobilization on a porous material helps to preserve the enzyme structure, thus improving the stability of the catalytically active protein.

## 2.2. Enzyme Binding Efficiency

The TiN nanostructured supports for enzyme immobilization with different morphological features have been synthesized by Pulsed Laser Deposition (PLD). During this synthesis process, a solid target of the material to be deposited is hit by a laser pulse. The high-energy pulse vaporizes the target and ionizes the as-formed vapor, creating a mixture of charged (plasma) and neutral atoms and molecules which expands at supersonic speed in the vacuum chamber. This partially ionized supersonic jet is called plume. If the plume interacts with a background gas during its expansion, its constituents aggregate in clusters and nanoparticles, which, in turn, are scattered from the axial direction and acquire a velocity component in a plane perpendicular to the direction of motion. As the plume impacts the substrates, atoms, clusters and nanoparticles self-assemble

in films the morphology of which depends on the different deposition parameters, as thoroughly discussed in other works.<sup>[55,56]</sup> To simplify, for any given set of laser parameters (fluence, spot size, repetition rate) and target-to-substrate distance, the deposition process is controlled by the pressure and nature of the background gas. In brief, as the pressure is increased, the structure of the deposit evolves from dense and compact towards a more nanostructured and porous one, as was observed for different materials, e.g. Al<sub>2</sub>O<sub>3</sub>,<sup>[57]</sup> WO<sub>3</sub>,<sup>[58]</sup> TiO<sub>2</sub>,<sup>[59]</sup> or MoS<sub>2</sub>.<sup>[60]</sup> Previous works have studied in detail the influence of the background gas on the PLD plasma dynamics<sup>[61,62]</sup> and the relationship of the kinetic energy of the plasma on the growth regime of the nanostructured films.<sup>[60,63]</sup>

Here we focus solely on the conditions leading to arrays of hierarchical nanostructures with a characteristic “nanotree” morphology, already demonstrated to be promising as catalyst support.<sup>[47]</sup> The evolution of the morphology and porosity features of the TiN support is visualized by the scanning electron microscope (SEM) micrographs shown in Figure 1a–c. The TiN nanostructured film synthesized at the lowest pressure of 30 Pa (TiN 30 Pa, Figure 1a) exhibits columnar elements with limited spacing and an overall compact morphology, because of the growth of the high kinetic energy of the plasma constituents during the growth of the deposit. Increasing the pressure to 45 Pa (TiN 45 Pa, Figure 1b) enhances the porosity of the film as the kinetic energy of the plasma diminishes, with larger spacing between the hierarchical columnar elements of the film. Lastly, for the highest gas pressure of 60 Pa (TiN 60 Pa, Figure 1c) the very low kinetic energy of the plasma and the growth of the nanostructure by the successive ‘soft’ landing of weakly-energetic particles leads to the formation of nanostructured aggregates with a ‘nanotree’ character, with higher

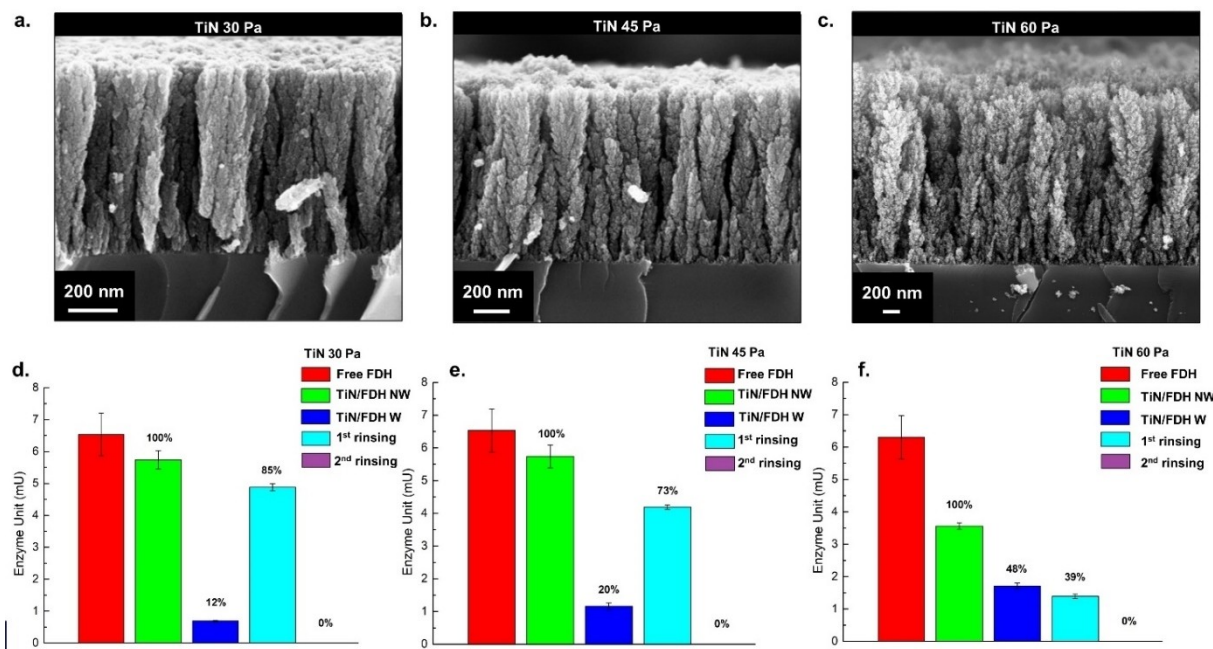


**Figure 1.** (Top) Cross section SEM images of TiN films deposited at different background gas pressures 30 Pa (a), 45 Pa (b) and 60 Pa (c). Bottom: Corresponding results of the enzyme assay.

porosity and pronounced internal spacing. In our previous work on the characterization of TiN hierarchical nanostructures, we confirmed this evolution in mesoscale morphology by BET (Brunauer-Emmett-Teller) surface area analysis and BJH (Barrett, Joyner, and Halenda) method for pore size distribution calculation.<sup>[47]</sup> Since in this study the same fabrication conditions for the TiN support are employed, we extend here our previous considerations on morphology. As the gas pressure changes from 30 Pa to 60 Pa, the BET surface area ranges from 135 m<sup>2</sup>g<sup>-1</sup> to 160 m<sup>2</sup>g<sup>-1</sup> with negligible variations with pressure, while the pore distribution of the nanostructured support drastically changes. Indeed, the mean pore size and the total pore volume of the nanostructure markedly increase, with the former ranging from  $\approx 16$  nm for TiN 30 Pa, to  $\approx 30$  nm for TiN 45 Pa up to  $\approx 46$  nm for the more porous TiN 60 Pa nanostructure. Notably, the TiN 60 Pa morphology exhibits a pore distribution uniform in volume, up to roughly 200 nm. The total pore volume, instead, roughly doubles in the transition from the more compact, TiN 30 Pa morphology to the more porous TiN 60 Pa nanostructure, ranging from  $\approx 0.23$  cm<sup>3</sup>g<sup>-1</sup> for the more compact structure to  $\approx 0.50$  cm<sup>3</sup>g<sup>-1</sup> for the more porous one. Moreover, increasing the gas pressure would lead to a more developed pore structure, with a larger fraction above 100–200 nm, but would compromise the mechanical stability of the TiN support: indeed, for an excessive gas pressure, the kinetic energy of the plasma constituents would be so low that the packing of the nanoparticles in the as-grown film would be extremely weak, critically worsening the mechanical properties of the film.<sup>[47]</sup> Consequently, pressures beyond 60 Pa are not considered in this study.

The effect of the distinct mesoscale morphologies of the TiN supports on the binding efficiency of the *TsFDH* enzyme is studied by synthesizing three different nanostructured supports (TiN 30 Pa, TiN 45 Pa and TiN 60 Pa) and assessing the binding through a 24 well format enzymatic assay, the results of which are summarized in Figure 1. The free form of the enzyme shows the largest enzyme unit (red bar in the histograms in Figure 1d–f), which indicates a faster reaction rate than the immobilized enzyme. We ascribe this phenomenon to the easier contact between the substrate and the enzyme when the *TsFDH* is free to diffuse in the solution.

Consequently, the enzyme unit calculated on the unrinsed TiN-immobilized *TsFDH* was set as the reference (100%, green bar in the histograms) to quantify the amount of specifically adsorbed protein after washing. With this choice, it is possible to directly correlate the enzyme unit registered for the rinsed TiN-immobilized *TsFDH* with the quantity of stably adsorbed enzyme, i.e. which is not lost with the rinsing procedure. Two successive rinsing procedures are performed to ensure the complete removal of the not-specifically adsorbed enzyme (light blue and violet bars in the histograms). Finally, the blue bars in the histograms in Figure 1 show the amount of *TsFDH* bound to the TiN nanostructures after the rinsing process, showing how the increased porosity of the TiN support is correlated to a higher percentage of immobilized and specifically adsorbed enzyme. For the more compact TiN 30 Pa film (Figure 1d), the percentage of stably adsorbed *TsFDH* is 12%,

which then increases to 30% for TiN 45 Pa (Figure 1e) and to 48% for the TiN 60 Pa support (Figure 1f). This last percentage corresponds to 1  $\mu$ g of specifically and stably adsorbed *TsFDH*: thus, the more porous TiN 60 Pa support is chosen as most suitable surface for the development of the bioelectrochemical system. Considering that the single *TsFDH* enzyme is immobilized to the surface by covalent interaction through any one or more site of the nanostructure-exposed Ti<sup>4+</sup> atoms, the enhanced adsorption is related to the mesoscale features of the TiN 60 Pa nanostructure. Indeed, this more porous TiN nanostructured support enhances the enzyme adsorption because it binds *TsFDH* not only on its outermost surface atoms but also on its internal pore structure. This effectively exposes the anchoring sites to the protein thanks to its large pore volume, large mean size and hierarchical nature, with uniform distribution in the 10–200 nm range, providing a more suitable microenvironment than a planar surface for the *TsFDH*.

Finally, we determined a calibration curve to assess the maximum binding capacity of the TiN 60 Pa support. Considering the high surface area and hierarchical pore size distribution of the nanostructure, we progressively increased the quantity of drop-casted enzyme until saturation of the exposed sites for the anchoring of the enzyme was achieved, thus maximizing the final enzyme loading efficiency. The assay was performed by drop-casting on the TiN 60 Pa support 30  $\mu$ l of a solution containing *TsFDH* at increasing concentrations, corresponding to the following *TsFDH* loadings: 2.1  $\mu$ g, 7.5  $\mu$ g, 15  $\mu$ g, 22.5  $\mu$ g, 34  $\mu$ g, 300  $\mu$ g and 1.14 mg. The resulting curve is plotted in Figure 2 and shows that, by increasing the concentration of the drop-casted *TsFDH*, the enzyme unit calculated on the TiN support after the rinsing process increases until a loading of 300  $\mu$ g is used. When 1.14 mg of *TsFDH* are deposited on TiN nanostructure, about 5% of the enzyme deposited is specifically adsorbed on the surface, corresponding to 59  $\mu$ g cm<sup>-2</sup> of immobilized enzyme.

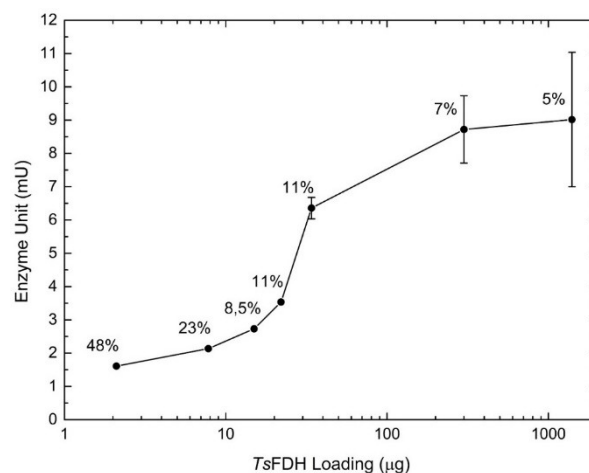


**Figure 2.** Saturation curves of the PLD-deposited TiN 60 Pa support as a function of the amount of *TsFDH* enzyme deposited. The percentage represent the ratio of bound enzyme on the TiN surface with respect to the drop-casted loading.

The enzyme unit curve displays a typical plateau profile, showing that for a drop-casted *TsFDH* loading of 1.14 mg, complete saturation of the surface anchoring sites of the TiN support is achieved. For this reason, the *TsFDH* quantity drop-casted on the TiN support for all electrochemical experiments was 1.14 mg, corresponding to an actual enzymatic loading of  $59 \mu\text{g cm}^{-2}$ . This analytical method represents a quantitative, robust and reproducible protocol for assessment of the amount of specifically-immobilized enzyme on a support, which here is used to evaluate the binding efficiency of the different TiN nanostructures.

## 2.3. Electrochemical Characterization

### 2.3.1. Electrochemical Stability of the TiN Support

Before assessing the  $\text{CO}_2$  reduction performance of the TiN-supported *TsFDH* enzyme, the electrochemical behavior and stability of the sole TiN 60 Pa support is investigated in the employed electrolyte (100 mM MES aqueous solution) in the operative potential window of the complete system. This assessment is done by cyclic voltammetry in the  $-1.15 V_{\text{RHE}}$ – $-0.55 V_{\text{RHE}}$  range. Figure 3, which reports the 20<sup>th</sup> voltammetry scan, shows that the TiN support does not catalyze any reaction in the cathodic potential sweep (i.e. between  $0 V_{\text{RHE}}$  and  $-1.15 V_{\text{RHE}}$ ), since no clear peak associable to any reduction reaction are found in the voltammogram.

However, as the applied potential becomes more cathodic, a reductive current is registered, which increases its value up to a maximum of approximately  $-2.3 \text{ mA cm}^{-2}_{\text{geo}}$  at  $-1.15 V_{\text{RHE}}$ . This current is due to the hydrogen evolution reaction (HER) from the TiN support, a side reaction always present to some extent in aqueous electrolytes because of it is thermodynamically favored over the  $\text{CO}_2$  reduction reaction in many catalysts. Despite the evolution of hydrogen, the TiN 60 Pa support shows no signs of degradation after the electrochemical operation in MES electrolyte in the applied potential range. Therefore, it is

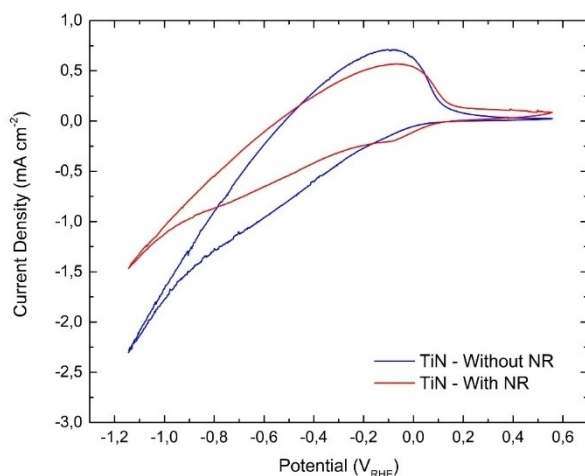


**Figure 3.** Electrochemical behaviour of the TiN support in the electrolyte employed for the  $\text{CO}_2$  reduction experiments.

considered stable for the application in the bioelectrochemical system. When neutral red is added to the system (red trace in Figure 3) a reduction peak is observed at approximately  $-0.1 V_{\text{RHE}}$ , which is ascribed to the recycling of  $\text{NADH}/\text{NAD}^+$  in the presence of neutral red, in accordance with previous studies.<sup>[42]</sup> Therefore, the stability of the TiN support is effectively assessed even in the complete electrocatalytic system employing a cofactor regeneration system.

### 2.3.2. $\text{CO}_2$ Reduction Performance Without NADH Regeneration System

After confirming the electrochemical stability of the TiN support, the  $\text{CO}_2$ -to-formate reduction performance of the complete TiN/*TsFDH* catalyst is analyzed by chronoamperometry measurements at fixed potentials ( $-0.15 V_{\text{RHE}}$ ,  $-0.45 V_{\text{RHE}}$ ,  $-0.75 V_{\text{RHE}}$ ) for three hours, firstly without employing any regeneration system for the NADH cofactor. Indeed, the first step in our performance evaluation is to assess the product selectivity and the electrochemical performance of the catalyst. A sacrificial electron donor for NADH regeneration is added to the system in a second moment and will be discussed in the next section.

The average Faradaic efficiency (FE) for  $\text{H}_2$  and formate of the TiN/*TsFDH* catalytic systems is reported in Figure 4.

The systems are characterized by a good stability in the chosen electrolyte under applied potential, since the current profiles registered in the chronoamperometries (Figure S1 4) are constant during the whole period of analysis. Comparable stabilities have been reported for similar systems, with chronoamperometries reported for durations ranging from 45 minutes for a *CbFDH* enzyme immobilized on a graphite-based cathode<sup>[44]</sup> to 5 hours for a free *CbFDH* coupled with a NADH/ $\text{NAD}^+$  regeneration system.<sup>[64]</sup> Furthermore, the three-hour stability at an applied potential of  $-0.75 V_{\text{RHE}}$  is a remarkable result, since this potential value is much larger than previously reported. Indeed, bioelectrochemical systems employing enzymes of the FDH family usually perform electrochemical testing applying potentials ranging approximately from  $+0.1 V_{\text{RHE}}$  to  $-0.45 V_{\text{RHE}}$ .<sup>[42–44,64]</sup>

The TiN 60 Pa support without any enzyme (blue trace in Figure 4) exhibits a 100% FE for  $\text{H}_2$  at all three applied potentials and does not produce any formate, confirming the qualitative considerations extrapolated from the cyclic voltammetry analysis. When the free form of the *TsFDH* enzyme is added to the system (TiN/*FDH* free, red trace in Figure 4), and is not adsorbed on the TiN support, the  $\text{CO}_2$ -to-formate reduction performance improves, with a 47% FE for formate at the lowest applied overpotential, which however drops to 2.5% at  $-0.45 V_{\text{RHE}}$  and  $\approx 0.6\%$  at  $-0.75 V_{\text{RHE}}$ . The selectivity towards  $\text{H}_2$  is high, with an  $\approx 82\%$  FE at  $-0.15 V_{\text{RHE}}$  with increases to 98% and 100% as the applied potential becomes more cathodic. The higher selectivity for  $\text{H}_2$  at increasingly cathodic potentials is explained through the faster HER kinetics than  $\text{CO}_2$  reduction, which at high overpotentials applied to the catalyst determines a faster adsorption and reduction of protons from the electro-

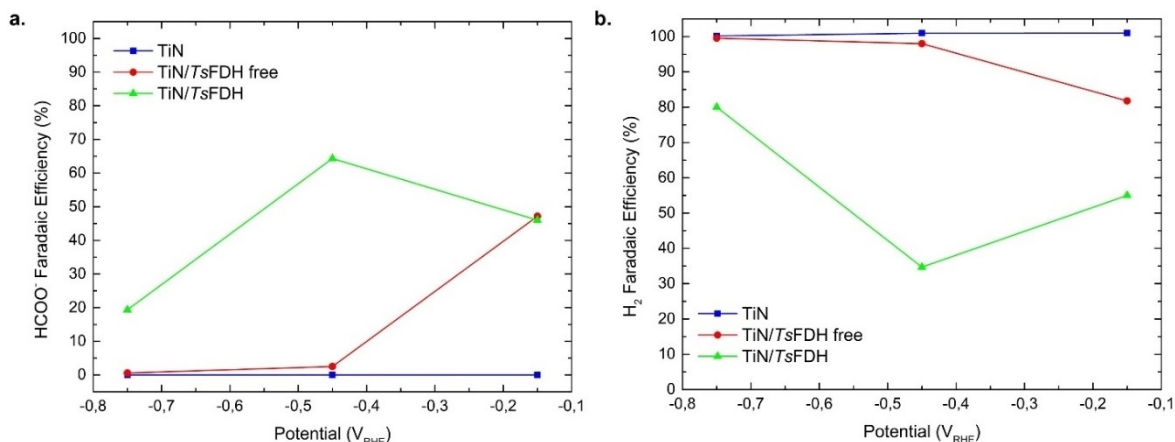


**Figure 4.** Mean Faradaic efficiency towards a. formate and b. hydrogen for the different BES, without any NADH regeneration system. TiN (blue trace) is the sole support without any enzyme. TiN/FDH free (red trace) employs the free form of the enzyme, dispersed in the electrolyte, and the TiN support as cathode. TiN/FDH (green trace) represents the FDH enzyme immobilized on the TiN surface.

lyte than CO<sub>2</sub>. At an applied potential of  $-0.15 V_{RHE}$ , the total FE of the TiN/FDH free system exceeds 100%: while H<sub>2</sub> production occurs by electrochemical reaction on the TiN support, reduction of CO<sub>2</sub> to HCOO<sup>-</sup> by the TsFDH enzyme occurs both by electrochemical reaction and by homogeneous catalysis. In fact, it is known that FDH enzymes can catalyze CO<sub>2</sub> reduction to HCOO<sup>-</sup> in the absence of an applied potential.<sup>[45,54,65]</sup> Consequently we ascribe the portion of FE for formic acid above 100% to CO<sub>2</sub> reduction by homogeneous catalysis of the free enzyme, dispersed in the electrolyte.

Lastly, the catalytic system comprising the TsFDH enzyme specifically adsorbed on the TiN support (TiN/FDH, green trace in Figure 4) exhibits a remarkable CO<sub>2</sub> reduction performance. A good selectivity towards HCOO<sup>-</sup> is observed, with higher FE values than the previous systems ranging from 46% at  $-0.15 V_{RHE}$  to 64% at  $-0.45 V_{RHE}$  and  $\approx 19.4\%$  at  $-0.75 V_{RHE}$ . This FE trend, characterized by a maximum at intermediate overpotential, is related to the competing CO<sub>2</sub>R and HER energy

profiles. At low overpotential ( $-0.15 V_{RHE}$ ), the lower activation energy of the HER than CO<sub>2</sub>R shifts the selectivity of the system towards hydrogen evolution. Nevertheless, the CO<sub>2</sub>R reaction pathway on the TsFDH active site is more energetically-favorable than CO<sub>2</sub> transition metal catalysts,<sup>[25]</sup> therefore mitigating this effect and resulting in a good FE for HCOO<sup>-</sup> of 46%. On the other hand, at high overpotential ( $-0.75 V_{RHE}$ ) the faster HER kinetics than CO<sub>2</sub>R favors hydrogen evolution,<sup>[66,67]</sup> whose FE increases to 80% at the expense of that for HCOO<sup>-</sup>. In fact, by increasing the overpotential, the gain associated to HER is proportional to kinetic rate constant, while CO<sub>2</sub>R depends to the kinetic parameters of TsFDH, slower at higher overpotentials. These two negative trends are minimized at intermediate overpotentials, where the CO<sub>2</sub>R selectivity is maximized.

Along with the system selectivity, the product yield is an important parameter for assessing the feasibility of the BES system, and is reported for H<sub>2</sub> and HCOO<sup>-</sup> in Figure 5. While the

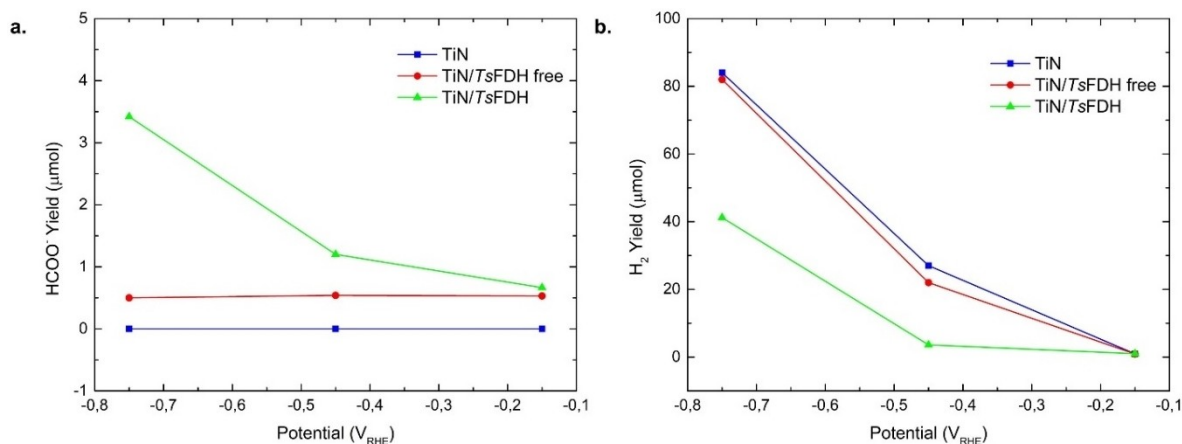


**Figure 5.** Mean yield of a. formate and b. hydrogen for the different BES, without any NADH regeneration system. TiN (blue trace) is the sole support without any enzyme. TiN/FDH free (red trace) employs the free form of the enzyme, dispersed in the electrolyte, and the TiN support as cathode. TiN/FDH (green trace) represents the FDH enzyme immobilized on the TiN surface.

formate yield for the TiN support and TiN/FDH free system is, respectively, zero and negligible, the production of formate drastically increases with the applied potential for the TiN/FDH system, reaching a maximum of 3.42  $\mu\text{mol}$  for  $-0.75 V_{\text{RHE}}$ .

### 2.3.3. CO<sub>2</sub> Reduction Performance with NADH Regeneration System

The remarkable performance registered for the bioelectrochemical system can be further improved by adding a regeneration system for the NADH cofactor. As schematized in Figure S1 2, CO<sub>2</sub> reduction on the TsFDH active site depends on the concomitant oxidation of NADH to NAD<sup>+</sup>. As the reaction proceeds over time, NADH is converted to NAD<sup>+</sup> and a smaller quantity of cofactor is available to the enzyme for CO<sub>2</sub> reduction, thus resulting in a slower reaction rate. This drawback can be overcome by adding to the BES a molecule that acts as electron donor and regenerates NADH, i.e. supporting

the reduction of the as-formed NAD<sup>+</sup> to NADH, as methyl viologen of neutral red (NR).<sup>[65,68]</sup> Here, the latter is added to the system as NADH regeneration system and the reduction performance system is evaluated again by repeating the chronoamperometries at  $-0.15 V_{\text{RHE}}$ ,  $-0.45 V_{\text{RHE}}$  and  $-0.5 V_{\text{RHE}}$  for a three-hour period, with the results being reported in Figure 6 and Figure 7. The stability of the catalytic system is also confirmed in the presence of neutral red, since the current profiles registered during the time-dependent measurements are stable, showing no visible sign of degradation of the bioelectrocatalytic system (Figure S1 5).

The system with the free enzyme in solution (TiN/FDH free/NR, dark cyan trace in Figure 6) exhibits the same behavior of the TiN/FDH free system without neutral red. A high selectivity towards H<sub>2</sub> is observed for the three applied potentials, with FE ranging from 94% to 100% and a low selectivity towards formate, with a 6% FE at  $-0.45 V_{\text{RHE}}$ . Again, the 23% FE for formate at the lowest potential brings the total FE of the system above 100%, because of the homogeneous catalysis of the

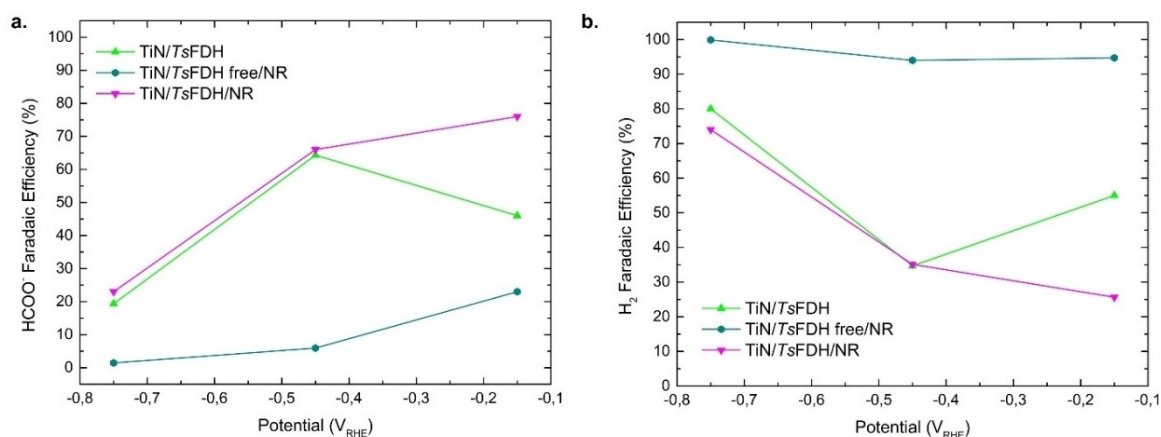


**Figure 6.** Mean Faradaic efficiency towards a. formate and b. hydrogen for the different BES, employing neutral red (NR) as NADH regeneration system. TiN/FDH free/NR (dark cyan trace) employs the enzyme in its free form, dispersed in the electrolyte along with neutral red. TiN/FDH/NR (magenta trace) represents the immobilized form of the enzyme on the TiN support, along with NR dispersed in the electrolyte.

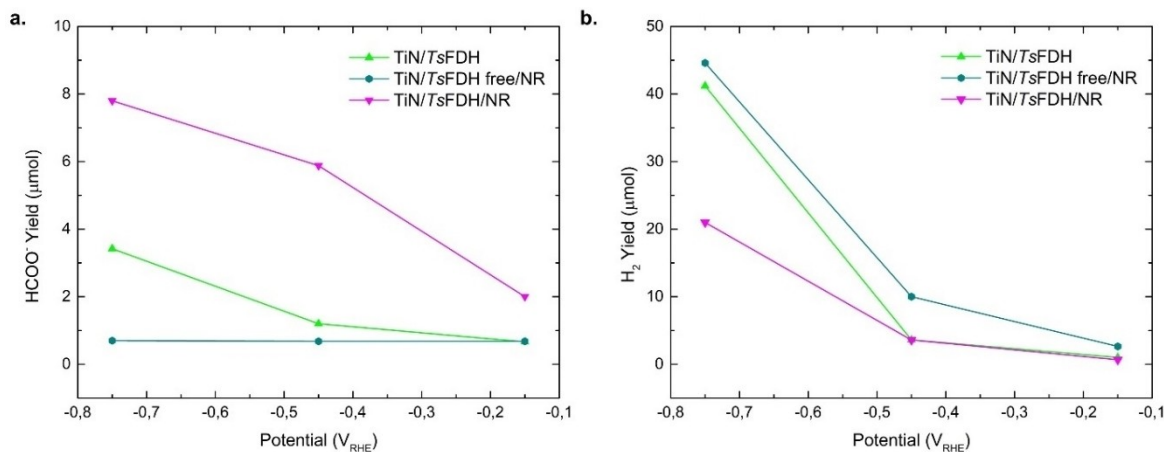


**Figure 7.** Mean yield of a. formate and b. hydrogen for the different BES, employing neutral red (NR) as NADH regeneration system. TiN/FDH free/NR (dark cyan trace) employs the enzyme in its free form, dispersed in the electrolyte along with neutral red. TiN/FDH/NR (magenta trace) represents the immobilized form of the enzyme on the TiN support, along with NR dispersed in the electrolyte.

enzyme in the electrolyte without the effect of the applied potential. The  $\text{HCOO}^-$  yield of the system remains low and independent on the potential, with a value of  $\approx 0.7 \mu\text{mol}$ , further supporting the idea of  $\text{CO}_2$  reduction by homogeneous catalysis. On the other hand, the  $\text{H}_2$  yield is very high and shows an exponential trend with the overpotential, suggesting that the main electrochemical reaction is HER by the support. When the enzyme is adsorbed on the TiN support instead (TiN/FDH/NR, magenta trace in Figure 6), a radical  $\text{CO}_2$  reduction performance improvement is registered. An improved selectivity towards  $\text{HCOO}^-$  with respect to the system without neutral red (TiN/FDH, green trace in Figure 6) is observed for all the applied potentials, with high FE values of 76% and 66% at  $-0.15 V_{\text{RHE}}$  and  $-0.45 V_{\text{RHE}}$  respectively, although at the highest overpotential the FE decreases to 23%. Similar to the TiN/FDH system, this selectivity trend is consistent with the energy profiles of the competing HER and  $\text{CO}_2\text{R}$ . The beneficial effect of neutral red on the catalytic efficiency of the enzyme is well described by the  $\text{HCOO}^-$  yield values, shown in Figure 7.

The productivity drastically improves thanks to the NADH regeneration system, with 4.9-fold and 2.3-fold improvements with respect to the TiN/FDH system without neutral red, at  $-0.45 V_{\text{RHE}}$  and  $-0.75 V_{\text{RHE}}$  respectively, achieving a maximum yield of  $7.8 \mu\text{mol}$  at the highest overpotential and confirming the beneficial effect on reaction rate and yield of the NADH regeneration system. Notably, the  $\text{H}_2$  yield at the highest overpotential is roughly halved when neutral red is added to the TiN/FDH system, further confirming the enhanced performance thanks to the NADH regeneration system. The drastic improvements in formate selectivity and product yield, with maximum values of  $7.8 \mu\text{mol}$  at  $-0.75 V_{\text{RHE}}$  and 76% at  $-0.15 V_{\text{RHE}}$  respectively, arises from the coupled effect of the nanostructured TiN support and the effective immobilization of the enzyme. Additionally, hydrogen productivity was minimized, in terms of low FE at low overpotentials and limited product yield at high overpotentials. When the two components are decoupled, the performance instead is worsened. The free form of the enzyme exhibits low yield ( $\approx 0.7 \mu\text{mol}$  over three hours of operation) and low FE for  $\text{CO}_2\text{R}$ . When instead the enzyme is absent from the system, the TiN support catalyzes with a 100% selectivity the HER. The incorporation of the NADH regeneration system in the electrolyte improved the  $\text{CO}_2$  reduction selectivity and yield, but the remarkable catalytic performance was present also with no NADH regeneration system.

## 2.4. Discussion

The product yield is a paramount criterion to assess the performance and the technological feasibility of the  $\text{CO}_2\text{R}$  application of FDH-based BES system. Consequently, we compare the performance of the TiN/TsFDH BES with other notable FDH-based  $\text{CO}_2$  reduction systems found in the literature, utilizing both NAD-dependent, aerobic FDHs and organometallic, oxygen-labile FDHs, extrapolating the gravimetric formate yield (measured in  $\mu\text{mol mg}_{\text{FDH}}^{-1} \text{h}^{-1}$ ) and employing

it as figure of merit. It is important to stress that the compared systems operate in different conditions (e.g. applied potential, pH and type of electrolyte, FDH type and NADH regeneration mechanism) which have a marked influence on the final performance and yield. For instance, the electrolyte pH influences the intrinsic activity of FDH,<sup>[69]</sup> while the concentration of the NADH/NAD<sup>+</sup> cofactor modifies the equilibrium of the FDH-catalyzed redox reaction, thus influencing the final productivity in the forward ( $\text{CO}_2$  reduction) and in the reverse (formate oxidation) reaction.<sup>[64]</sup> These differences must be considered when comparing the different BES systems; however, qualitative considerations and comparisons can surely be made.

BES systems employing NAD-dependent enzymes in their free form, with or without the application of an electrical potential, are characterized by gravimetric yields ranging from  $0.02 \mu\text{mol mg}_{\text{FDH}}^{-1} \text{h}^{-1}$ , achieved by a free CbFDH utilizing methylviologen as  $\text{e}^-$  carrier,<sup>[70]</sup> to  $4.4 \mu\text{mol mg}_{\text{FDH}}^{-1} \text{h}^{-1}$  registered for a BES system exploiting as catalyst a free CbFDH enzyme and a graphite-based cathode as working electrode.<sup>[42]</sup> A remarkable productivity ( $55.3 \mu\text{mol}_{\text{formate}} \text{h}^{-1}$ ) was reported for a BES employing a free, NAD-dependent FDH coupled with a graphene-based photocatalyst for NADH regeneration,<sup>[71]</sup> although, since the loading was reported in enzyme units, the extrapolation of the gravimetric yield was not performed because it would have introduced an excessive uncertainty in converting the loading from units to milligrams. The optimized TiN/TsFDH BES, on the other hand, exhibits a remarkable gravimetric formate yield, with a value as high as  $44.1 \mu\text{mol mg}_{\text{FDH}}^{-1} \text{h}^{-1}$  (Figure SI 6), outperforming these systems with the free form of the enzyme. Even if, as observed in previous work, the random orientation of the enzymes on the surface after the immobilization may limit the accessibility of the reactants to the active sites,<sup>[44,72]</sup> the final activity and stability achieved by the TiN/TsFDH system are markedly enhanced by the presence of the support, outperforming by at least one order of magnitude the best-performing BES systems with free NAD-dependent FDH and registering a tenfold improvement in gravimetric yield with respect to the free TsFDH.<sup>[54]</sup> Notably, the utilization of the nanostructured TiN scaffold allows to drastically decrease the enzymatic loading, from tens of mg typical of free enzyme systems to hundreds or tens of micrograms of the immobilized system, diminishing the time and costs associated to the expression and purification of the enzyme.

Immobilization of the NAD-dependent enzymatic catalyst on an inorganic support has proven to be an efficient method to improve the stability of the organic compound of the BES. Consequently, the catalytic activity of the system usually exhibits higher product yields. In this regard, a CbFDH enzyme adsorbed on a polystyrene-based support, where a Cu foam electrode was used for NADH regeneration, registered a gravimetric formate yield of  $1.6 \mu\text{mol mg}_{\text{FDH}}^{-1} \text{h}^{-1}$  and showed a much longer stability than the free enzyme.<sup>[72]</sup> Nevertheless, in these systems the inorganic support is mainly employed as electrode for the *in-situ* regeneration of the NADH/NAD<sup>+</sup> cofactor, which is a critical technological aspect to be addressed towards the efficient application of this technology. Conse-



quently, in these cases the coupling between support and enzymatic catalyst is not optimized, limiting the electrocatalytic activity of the NAD-dependent FDH. A BES employing a flat graphite substrate for the immobilization of a CbFDH catalyst and for regeneration of the NADH cofactor, occurring thanks to polymerized neutral red electrodeposited on the electrode, registered a gravimetric formate yield of  $28.7 \mu\text{mol mg}_{\text{FDH}}^{-1} \text{h}^{-1}$ .<sup>[43]</sup> Nevertheless, due to this double role of the electrode in the BES, only a fraction of this yield was due to the electroreduction of  $\text{CO}_2$  to  $\text{HCOO}^-$  by the immobilized FDH. Indeed, when the same enzyme was supported, employing Nafion micelles for immobilization, on a graphite electrode modified with electrodeposited, polymerized neutral red for NADH regeneration,<sup>[46]</sup> a gravimetric formate yield of  $30.1 \mu\text{mol mg}_{\text{FDH}}^{-1} \text{h}^{-1}$  was observed, although only  $11.3 \mu\text{mol mg}_{\text{FDH}}^{-1} \text{h}^{-1}$  were produced *via* electrochemical  $\text{CO}_2$  reduction by the FDH. Similarly, immobilization of a CbFDH enzyme on a graphite-PTFE (polytetrafluoroethylene)-based electrode, exploiting electrodeposited polymerized neutral red as electron mediator and a carbonic anhydrase enzyme to enhance the solubility of gaseous  $\text{CO}_2$  in the electrolyte,<sup>[44]</sup> improved the stability of the enzymatic component with respect to its free form and the productivity of the system. Nevertheless, the inorganic support was optimized for NADH recycling while its selectivity towards formate was limited, with an FE of 8.4% against an FE of 91.6% towards NADH/NAD<sup>+</sup> interconversion, corresponding to a gravimetric yield of  $0.02 \mu\text{mol mg}_{\text{FDH}}^{-1} \text{h}^{-1}$  of formate produced by  $\text{CO}_2$  electroreduction.

On the other hand, in the TiN/TsFDH BES the coupling between inorganic support and enzyme is optimized to maximize the electrocatalytic activity of the catalyst. In this way, the system achieves a state-of-art gravimetric formate yield ( $44.1 \mu\text{mol mg}_{\text{FDH}}^{-1} \text{h}^{-1}$ ), the highest value for BES systems employing supported, NAD-dependent FDH, as well as a remarkable stability under applied potential during a 3-hour operation and an impressive formate FE up to 76%, marked improvements with respect to the CbFDH-based BES system with the highest product yield. The impressive efficiency of the TiN/TsFDH system highlights the paramount importance for enhancing the  $\text{CO}_2$  electroreduction efficiency of BES systems of precise morphology control and the nano-engineering of the support for enzyme immobilization. Indeed, the implementation of the nanostructured, hierarchical TiN support leads to an optimization of enzyme loading and immobilization mechanism, to an enhancement in enzyme stability and to an increased activity, outperforming flat supports in terms of efficiency of electrochemical reduction of  $\text{CO}_2$  to  $\text{HCOO}^-$  by the enzymatic catalyst.

The importance of a precise structural control for the scaffold emerges also when the productivity of BES employing supported, oxygen-labile FDHs is analyzed, where mesoscale morphology of the immobilization support drastically affects the performance of the resulting BES. When coupled with supports with tailored pore profile, like mesoporous  $\text{TiO}_2$ <sup>[38]</sup> or inverse-opal  $\text{TiO}_2$ ,<sup>[39]</sup> a W-containing FDH showed an impressive productivity, with gravimetric yields of  $241.8 \mu\text{mol mg}_{\text{FDH}}^{-1} \text{h}^{-1}$

for the former support or  $65.6 \mu\text{mol mg}_{\text{FDH}}^{-1} \text{h}^{-1}$  for the latter. Analogously, a Mo-containing FDH exhibited a  $26.4 \mu\text{mol mg}_{\text{FDH}}^{-1} \text{h}^{-1}$  yield, thanks to the enhanced electron transfer granted by a complex cobaltocene-modified poly(ethylenimine) support.<sup>[73]</sup> Despite the much higher  $\text{CO}_2$  reduction activity of organometallic FDHs, with a turnover frequency 3–4 orders of magnitude higher than that of NAD-dependent FDHs, these productivity values are comparable with those of the optimized BES systems employing supported, oxygen-tolerant FDHs. Indeed, when the employed support has a limited nano-engineered morphology, the utilization of the immobilized enzyme can be inefficient, leading to a reduced catalytic activity, suboptimal electron and mass transfer to the reaction active site, and limited productivity of the resulting BES system. On the other hand, coupling the enzyme with nano-engineered supports with complex mesoscale morphologies benefits the final catalytic efficiency. It enhances the binding of the enzyme to the inorganic support and allows an efficient utilization of the catalyst and improves the availability of reactants to the enzyme active site.

### 3. Conclusions

In this work, we developed a proof-of-concept hybrid BES system for  $\text{CO}_2$  electroreduction to formate. For this purpose, a novel nanostructured TiN support by PLD with high surface area and hierarchical pore profile was used to immobilize a TsFDH enzymatic catalyst. The optimal TiN support morphology for immobilization was found to be the one with a uniform pore distribution in the 10 nm–200 nm range, which allowed for enzyme adsorption not only on the outermost surface but also on its internal pore structure, as well as for a precise tuning of the loading of specifically-immobilized enzyme on the support. The resulting BES system exhibits a remarkable  $\text{CO}_2$  reduction performance, with a maximum formate FE of 76% at  $-0.15 \text{ V}_{\text{RHE}}$  and a gravimetric product yield as high as  $44.1 \mu\text{mol mg}_{\text{FDH}}^{-1} \text{h}^{-1}$  at  $-0.75 \text{ V}_{\text{RHE}}$ .

The remarkable results achieved by this BES exploiting a supported, oxygen-tolerant FDH show the critical importance of implementing complex supports precisely engineered for enzyme immobilization, with an internal pore profile tailored to the characteristics of the enzyme. In this way, resulting BES performance can be drastically improved in terms of catalyst loading, binding efficiency, and enzyme activity with respect to usually employed immobilization supports for NAD-dependent FDHs. Indeed, these surfaces are usually exploited to enable the *in-situ* regeneration of the NADH/NAD<sup>+</sup> cofactor and their morphology and surface composition are not optimized for enzyme immobilization. This leads to a suboptimal utilization and activity of the enzymatic catalyst, negatively affecting the reduction performance. Differently, the implementation of a nanostructured TiN support realizes an efficient coupling between scaffold and catalyst, reaching performances comparable to – or close to – BES systems employing organometallic FDHs, despite the much higher intrinsic activity of these enzymes. Therefore, our proof-of-concept BES represents an

important and promising step in the systematic implementation of nano-engineered supports with a tailored internal structure for immobilization of oxygen-tolerant FDHs, moving these catalytic systems closer to their technological feasibility and to matching the performance of organometallic FDHs, in the framework of the widespread utilization of this technology.

## Materials and Method

### TiN Nanostructured Support Fabrication

Titanium nitride nanostructured supports are synthesized *via* Pulsed Laser Deposition, following the same procedure outlined in a previous work by our group.<sup>[47]</sup> A crystalline titanium nitride (99.95%, Testbourne) target is ablated by UV laser pulses coming from an excimer laser (Coherent GmbH COMPex 205 F,  $\lambda = 248$  nm, repetition rate 20 Hz) with an incident fluence of  $3.4 \text{ J cm}^{-2} \text{ pulse}^{-1}$ . The substrates for the deposition were placed parallel to the target, offset with respect to the center of the target, at a distance of 5 cm. Step-motors (Mitsubishi) imposed a roto-translation motion to the target and a rotation motion to the substrate during the ablation through home-made software. Mirror-polished glassy carbon (Tokai carbon) and soda lime glass slides (Thermo Fisher Scientific) were used to grow the TiN nanostructures for electrochemical experiments and study the immobilization of the enzyme on the catalyst, respectively. Before, the substrates were sonicated in acetone (Honeywell), isopropanol (Honeywell) and distilled water. PLD takes place in a stainless-steel vacuum chamber (Kenosistec PI350), evacuated to a base vacuum of  $\sim 0.003$  Pa and then filled with a  $\text{N}_2/\text{H}_2$  (95%/5%) background gas up to the desired pressure. Three different background gas pressure, namely 30 Pa (TiN 30 Pa), 45 Pa (TiN 45 Pa) and 60 Pa (TiN 60 Pa), were employed for the synthesis of the TiN nanostructures. For each background gas pressure, the number of pulses was adjusted to deposit a  $1 \mu\text{m}$ -thick nanostructure.

### Expression and Purification of TsFDH

The full-length FDH gene (residues 1 to 401) from *Thiobacillus sp. strain KNK65MA* was cloned into a pET23a(+) vector with a C-terminal hexaistidine-tag (GenScript, USA) and transformed into competent *E. coli* BL21 ( $\lambda$ DE3) pLysS cells (Novagen, USA). TsFDH was expressed and purified as described elsewhere.<sup>[74]</sup> Briefly, cells were cultured at  $37^\circ\text{C}$  in 1 liter of Luria-Bertani (LB) broth (plus ampicillin) until the  $\text{OD}_{600}$  reached 0.6. Then, overnight protein expression at  $20^\circ\text{C}$  was induced by adding isopropyl 1-thio- $\beta$ -D-galactopyranoside (Sigma Aldrich) to a final concentration of 1 mM. Cells were then collected by centrifugation and resuspended in buffer A (50 mM sodium phosphate pH 7.1, 200 mM NaCl). After sonication, the soluble fraction was loaded onto a Ni-NTA (Qiagen) column equilibrated with buffer A. Column was washed with buffer A containing 40 mM imidazole, then TsFDH was eluted with the same buffer supplemented with 400 mM. Protein-containing fraction was pooled, concentrated and loaded onto a Sephacryl 100 HR HiPrep 26/60 size exclusion column (GE Healthcare) pre-equilibrated with buffer A. The resulting protein was concentrated to  $\sim 12$  mg/ml and stored at  $-80^\circ\text{C}$ . The purity of TsFDH ( $>98\%$ ) was confirmed by 12% SDS-PAGE (Figure S1 1). Protein concentration was estimated by Bradford protein assay using bovine serum albumin as standard. All the purification steps described above were performed at room temperature.

### Enzymatic Activity Assay

TsFDH activity was determined using a Spark 10 M (Tecan) microplate reader, utilizing a continuous assay that detects the reduction of  $\beta$ -nicotinamide adenine dinucleotide ( $\text{NAD}^+$ ) to NADH at 340 nm ( $\text{NADH } \epsilon_{340} = 6220 \text{ M}^{-1} \text{ cm}^{-1}$ ) caused by the oxidation of formic acid to  $\text{CO}_2$ , similarly as described elsewhere.<sup>[54]</sup> The  $200 \mu\text{L}$  reaction mixture contained 50 mM MES buffer pH 6.1,  $0.025 \text{ mg mL}^{-1}$  TsFDH, 3 mM  $\text{NAD}^+$  and 80 mM  $\text{HCOONa}$ . A background reading was performed before initiating the reaction by addition of TsFDH. The assay was adapted to support a 96 well format. One enzyme unit (U) is defined as the amount of enzyme required to produce  $1 \mu\text{mol}$  of product (NADH) per minute and specific activity is expressed as  $\text{U mg}^{-1}$ . In all the listed experiments, the results are the mean values of three replicates.

### Enzyme Stability

Stability studies for the enzyme in solution were performed as follows. A solution of  $0.07 \text{ mg mL}^{-1}$  TsFDH in 50 mM MES pH 6.1 was incubated at  $25^\circ\text{C}$ . Then, at regular periods, aliquots were withdrawn and residual activity was immediately measured, according to the assay described in the previous section.

### TsFDH Immobilization on TiN Support and Binding Efficiency

TsFDH was prepared in 100 mM MES pH 6.1 to the concentration of  $0.07 \text{ mg mL}^{-1}$ . Ultrapure water (Milli-Q Direct 8 Water Purification System) was employed for solution preparation. Then,  $30 \mu\text{L}$  of this solution (total TsFDH loading of  $2.1 \mu\text{g}$ ) was drop-casted onto a TiN surface (active area  $1 \text{ cm}^2$ ) and air-dried for 30 minutes at room temperature. To evaluate the binding efficiency, the TsFDH activity was determined using the assay described above adapted for a 24 well plate format, with minimal modifications. The enzyme-modified electrodes were rinsed twice (10 minute each wash) in 1 mL reaction mixture containing 50 mM MES buffer pH 6.1 and 3 mM  $\text{NAD}^+$ . Then, the surface was deposited on the well bottom, and 1 mL of the reaction mixture was dropped onto the rinsed surface. The same setup was used to prepare a control electrode (not rinsed TiN/TsFDH) which was tested directly after the drop-casting and the air-drying process. Following a 1-minute incubation, the enzymatic reaction was started by adding  $\text{HCOONa}$  (Sigma-Aldrich) to a final concentration of 20 mM. Enzyme activity was determined by monitoring the cofactor absorbance variation at 340 nm during the oxidation reaction and the enzyme unit was calculated. The comparison between the enzymatic unit ( $\mu\text{mol min}^{-1}$ ) of these two enzyme-modified electrodes allowed the quantification of the amount of TsFDH that was efficiently adsorbed and catalytically active on the rinsed TiN surface. To optimize the immobilization procedure, and determine the saturation level of the TiN support, experiments have been performed by varying the drop-casted enzyme concentration, ranging from  $0.07 \text{ mg mL}^{-1}$  to  $38 \text{ mg mL}^{-1}$ . As control experiments, a blank TiN nanostructured support with no drop-casted enzyme (negative control) and a free form of TsFDH (positive control) were also analyzed. An overview of the experiment set up is shown in Figure 1. The same procedure was applied to evaluate three TiN nanostructures with different morphologies and porosities (TiN 30 Pa, TiN 45 Pa, TiN 60 Pa) to assess the relationship between the amount of adsorbed and active TsFDH and the porosity of the TiN nanostructure.

### Electrochemical Characterization

The  $\text{CO}_2$ -reducing activity of the TiN/TsFDH system was carried out in the bioelectrochemical system whose details are reported in

Table SI 1. Experiments were carried out in a single-compartment electrochemical cell where the electrochemical performance of *TsFDH* immobilized on TiN nanostructure and *TsFDH* free in electrolyte solution were compared. For each experimental study, the working electrode was composed of 59  $\mu\text{g}$  of immobilized or free enzyme and TiN electrode with an active area of  $1\text{ cm}^2$  while a platinum wire and an Ag/AgCl (saturated KCl) electrode were used as the counter and the reference electrode, respectively. A 100 mM MES (2-(*N*-morpholino)ethanesulfonic acid) pH 6.1 buffer solution (Sigma Aldrich) was used as the electrolyte with a total volume of 40 mL and 3 mM NADH (Sigma Aldrich) was required as *TsFDH* cofactor to enable the reduction reaction. The optimization of BES electrochemical reduction performance was realized by adding the reaction mix of 0.5 mM neutral red (NR) (Sigma Aldrich) to enable the cofactor recycling and thus promoting the  $\text{CO}_2$  reduction reaction. Before starting the measurements, the electrode was saturated by bubbling  $\text{CO}_2$  (99.99%, Rivoira) into the solution for 45 minutes. Continuous  $\text{CO}_2$  bubbling into the electrolyte at a constant flow rate of  $20\text{ mL min}^{-1}$  and stirring of the solution were maintained during the electrochemical experiments. The  $\text{CO}_2$  reduction performance of the electrode was assessed by using chronoamperometry measurements carried out for 3 hours at three applied potentials, viz.,  $-0.15\text{ V}_{\text{RHE}}$ ,  $-0.45\text{ V}_{\text{RHE}}$ ,  $-0.75\text{ V}_{\text{RHE}}$ . The TiN support stability in the electrolyte was assessed by performing 20 CV scans at a scan rate of  $20\text{ mVs}^{-1}$ , sweeping the potential in a range between  $-1.15\text{ V}_{\text{RHE}}$  and  $0.55\text{ V}_{\text{RHE}}$ . All the electrochemical measurements were performed with an Autolab Multi-Autolab M204 potentiostat. All potentials are reported against RHE, utilizing the Nerst equation for conversion:  $V_{\text{RHE}} = V_{\text{Ag/AgCl}} + 0.197 + 0.0591\text{ pH}$ .

### Product Analysis

Production of formic acid from the bioelectrochemical reduction of  $\text{CO}_2$  was evaluated by 500 MHz  $^1\text{H}$  NMR spectroscopy (Bruker Cryoprobe Avance 500 Neo). At the end of each 3-hour-long chronoamperometric experiment, electrolyte samples were collected and analyzed. The quantity of formic acid in each sample was calculated by comparing the area of the  $\text{HCOO}^-$  peak in NMR spectra with the peak area of a reference  $\text{HCOONa}$  at known concentration. Gas-phase products were analyzed online via a Varian Gas Chromatograph equipped with a capillary column (Varian CP SIL 5CB, 30 m long, 0.32 mm i.d.) and a PFPD detector. During the chronoamperometric measurements for gas-phase analysis, a constant  $\text{CO}_2$  flow rate of  $20\text{ mL min}^{-1}$  was maintained to saturate the electrolyte and the gas outlet samples were collected periodically and analyzed by the gas chromatograph. Finally, the Faraday efficiency (FE) for the electrosynthesis of reaction products was calculated as follows:

$$FE_i = \frac{z_i F n_i}{\int_0^t I dt} \times 100\%$$

where  $z_i$  is the number of electrons transferred for the formation of one molecule of product  $i$ ,  $n_i$  represents the moles of product  $i$ ,  $I$  is the reduction current intensity and  $t$  is the reaction time.

### Supporting Information

The Supporting Information contains additional details on SDS page analysis, chronoamperometric measurements and product yield, and performance comparison.

### Acknowledgements

All authors contributed to the conceptualization, to the experiments and to the writing of this paper.

### Conflict of Interest

The authors declare no conflict of interest.

**Keywords:** bioelectrochemical system · hybrid electrode ·  $\text{CO}_2$  reduction · formate dehydrogenase · nanostructured titanium nitride

- [1] L. Zhang, Z. J. Zhao, J. Gong, *Angew. Chem. Int. Ed.* **2017**, *56*, 11326.
- [2] D. Voiry, H. S. Shin, K. P. Loh, M. Chhowalla, *Nat. Chem. Rev.* **2018**, *2*, 0105, DOI 10.1038/s41570-017-0105.
- [3] S. Nitopi, E. Bertheussen, S. B. Scott, X. Liu, A. K. Engstfeld, S. Horch, B. Seger, I. E. L. Stephens, K. Chan, C. Hahn, J. K. Nørskov, T. F. Jaramillo, I. Chorkendorff, *Chem. Rev.* **2019**, *119*, 7610.
- [4] Y. Hori, in *Handb. Fuel Cells*, **2010**, pp. 1–14.
- [5] K. P. Kuhl, E. R. Cave, D. N. Abram, T. F. Jaramillo, *Energy Environ. Sci.* **2012**, *5*, 7050.
- [6] A. A. Peterson, F. Abild-Pedersen, F. Studt, J. Rossmeisl, J. K. Nørskov, *Energy Environ. Sci.* **2010**, *3*, 1311.
- [7] P. De Luna, R. Quintero-Bermudez, C.-T. Dinh, M. B. Ross, O. S. Bushuyev, P. Todorović, T. Regier, S. O. Kelley, P. Yang, E. H. Sargent, *Nat. Catal.* **2018**, *1*, DOI 10.1038/s41929-017-0018-9.
- [8] J. Qiao, Y. Liu, F. Hong, J. Zhang, *A Review of Catalysts for the Electroreduction of Carbon Dioxide to Produce Low-Carbon Fuels*, **2014**.
- [9] B. Khezri, A. C. Fisher, M. Pumera, *J. Mater. Chem. A* **2017**, *5*, 8230.
- [10] A. Klinkova, P. De Luna, C. T. Dinh, O. Voznyy, E. M. Larin, E. Kumacheva, E. H. Sargent, *ACS Catal.* **2016**, *6*, 8115.
- [11] X. Zheng, P. De Luna, F. P. García de Arquer, B. Zhang, N. Becknell, M. B. Ross, Y. Li, M. N. Banis, Y. Li, M. Liu, O. Voznyy, C. T. Dinh, T. Zhuang, P. Stadler, Y. Cui, X. Du, P. Yang, E. H. Sargent, *Joule* **2017**, *1*, 794.
- [12] J. P. Jones, G. K. S. Prakash, G. A. Olah, *Isr. J. Chem.* **2014**, *54*, 1451.
- [13] S. Hernández, M. Amin Farkhondeh, F. Sastre, M. Makkee, G. Saracco, N. Russo, *Green Chem.* **2017**, *19*, 2326.
- [14] T. Hatsukade, K. P. Kuhl, E. R. Cave, D. N. Abram, T. F. Jaramillo, *Phys. Chem. Chem. Phys.* **2014**, *16*, 13814.
- [15] Y. Huang, A. D. Handoko, P. Hirunsit, B. S. Yeo, *ACS Catal.* **2017**, *7*, 1749.
- [16] M. Schreier, Y. Yoon, M. N. Jackson, Y. Surendranath, *Angew. Chem. Int. Ed.* **2018**, *57*, 10221.
- [17] M. G. Kibria, C.-T. Dinh, A. Seifitokaldani, P. De Luna, T. Burdyny, R. Quintero-Bermudez, M. B. Ross, O. S. Bushuyev, F. P. García de Arquer, P. Yang, D. Sinton, E. H. Sargent, *Adv. Mater.* **2018**, *30*, 1804867.
- [18] A. ElMekawy, H. M. Hegab, G. Mohanakrishna, A. F. Elbaz, M. Bulut, D. Pant, *Bioresour. Technol.* **2016**, *215*, 357.
- [19] J. E. G. A. Rajales, A. L. B. U. Ilva, P. I. C. Harruau, *mBio* **2010**, *1*, e00103.
- [20] S. Bajracharya, K. Vanbroekhoven, C. J. N. Buisman, D. P. B. T. B. Strik, D. Pant, *Faraday Discuss.* **2017**, *202*, 433.
- [21] P. Deepak, G. van Bogaert, L. Diels, K. Vanbroekhoven, *A comparative assessment of bioelectrochemical systems and enzymatic fuel cells in the book "Microbial biotechnology: energy and environment"* edited by R. Arora and published by CAB International, **2012**, pp. 39–57.
- [22] P. Majumdar, D. Pant, S. Patra, *Trends Biotechnol.* **2017**, *35*, 285.
- [23] T. W. Woolerton, S. Sheard, Y. S. Chaudhary, F. A. Armstrong, *Energy Environ. Sci.* **2012**, *5*, 7470.
- [24] C. Santoro, C. Arbizzani, B. Erable, I. Ieropoulos, *J. Power Sources* **2017**, *356*, 225.
- [25] R. Kortlever, J. Shen, K. J. P. Schouten, F. Calle-Vallejo, M. T. M. Koper, *J. Phys. Chem. Lett.* **2015**, *6*, 4073.
- [26] J. Kim, H. Jia, P. Wang, *Biotechnol. Adv.* **2006**, *24*, 296.
- [27] X. Dominguez-benetton, S. Srikanth, Y. Satyawali, K. Vanbroekhoven, D. Pant, *J. Microb. Biochem. Technol.* **2013**, *56*, 007, DOI 10.4172/1948-5948.S6-007.
- [28] A. A. Peterson, J. K. Nørskov, *J. Phys. Chem. Lett.* **2012**, *3*, 251.
- [29] P. K. Addo, R. L. Arechederra, S. D. Minter, *Electroanalysis* **2009**, *22*, 807.

- [30] F. S. Baskaya, X. Zhao, M. C. Flickinger, P. Wang, *Appl. Biochem. Biotechnol.* **2010**, *162*, 391.
- [31] T. Reda, C. M. Plugge, N. J. Abram, J. Hirst, *Proc. Nat. Acad. Sci.* **2008**, *105*, 10654.
- [32] J. E. Cone, R. Martin, D. E. L. Rio, J. O. E. N. Davis, T. C. Stadtman, *Proc. Nat. Acad. Sci.* **1976**, *73*, 2659.
- [33] A. Graentzdoerffer, D. Rauh, A. Pich, J. R. Andreesen, *Arch. Microbiol.* **2003**, *179*, 116.
- [34] A. Idris, A. Bukhari, *Biotechnol. Adv.* **2012**, *30*, 550.
- [35] Y. Chen, P. Li, H. Noh, C. W. Kung, C. T. Buru, X. Wang, X. Zhang, O. K. Farha, *Angew. Chem. Int. Ed.* **2019**, *58*, 7682.
- [36] V. Vamvakaki, N. A. Chaniotakis, *Biosens. Bioelectron.* **2007**, *22*, 2848.
- [37] S. Datta, L. R. Christena, Y. R. S. Rajaram, *3 Biotech* **2013**, *3*, 1.
- [38] M. Miller, W. E. Robinson, A. R. Oliveira, N. Heidary, N. Kornienko, J. Warnan, I. A. C. Pereira, E. Reisner, *Angew. Chem. Int. Ed.* **2019**, *58*, 4601.
- [39] K. P. Sokol, W. E. Robinson, A. R. Oliveira, J. Warnan, M. M. Nowaczyk, A. Ruff, I. A. C. Pereira, E. Reisner, *J. Am. Chem. Soc.* **2018**, *140*, 16418.
- [40] S. K. Kuk, K. Gopinath, R. K. Singh, T. D. Kim, Y. Lee, W. S. Choi, J. K. Lee, C. B. Park, *ACS Catal.* **2019**, *9*, 5584.
- [41] K. Sakai, Y. Kitazumi, O. Shirai, K. Takagi, K. Kano, *Electrochem. Commun.* **2016**, *73*, 85.
- [42] S. Srikanth, M. Maesen, X. Dominguez-Benetton, K. Vanbroekhoven, D. Pant, *Bioresour. Technol.* **2014**, *165*, 350.
- [43] L. Zhang, J. Liu, J. Ong, S. F. Y. Li, *Chemosphere* **2016**, *162*, 228.
- [44] S. Srikanth, Y. Alvarez-Gallego, K. Vanbroekhoven, D. Pant, *ChemPhysChem* **2017**, *18*, 3174.
- [45] H. Choe, J. M. Ha, J. C. Joo, H. Kim, H. J. Yoon, S. Kim, S. H. Son, R. M. Gengan, S. T. Jeon, R. Chang, K. D. Jung, Y. H. Kim, H. H. Lee, *Acta Crystallogr. Sect. D* **2015**, *71*, 313.
- [46] L. Zhang, J. Ong, J. Liu, S. F. Y. Li, *Renewable Energy* **2017**, *108*, 581.
- [47] A. Perego, G. Giuffredi, P. Mazzolini, M. Colombo, R. Brescia, M. Prato, D. C. Sabarirajan, I. V. Zenyuk, F. Bossola, V. Dal Santo, A. Casalegno, F. Di Fonzo, *ACS Appl. Mater. Interfaces* **2019**, *2*, DOI 10.1021/acsaem.8b02030.
- [48] B. Avasarala, P. Haldar, *Int. J. Hydrogen Energy* **2011**, *36*, 3965.
- [49] R. Kröger, M. Eizenberg, C. Marcadal, L. Chen, *J. Appl. Phys.* **2002**, *91*, 5149.
- [50] V. Lingwal, N. S. Panwar, *J. Appl. Phys.* **2005**, *97*, 104902, DOI 10.1063/1.1896433.
- [51] I. Miloš, H.-H. Strehblow, B. Navinšek, M. Metikoš-Huković, *Surf. Interface Anal.* **1995**, *23*, 529.
- [52] B. Avasarala, P. Haldar, *Electrochim. Acta* **2010**, *55*, 9024.
- [53] Y. Ju, T. Chen, Z. Wu, Y. Jiang, *Adv. Condens. Matter Phys.* **2013**, *33*, 676.
- [54] H. Choe, J. C. Joo, D. H. Cho, M. H. Kim, S. H. Lee, K. D. Jung, Y. H. Kim, *PLoS One* **2014**, *9*, 14.
- [55] R. Eason, *Pulsed Laser Deposition of Thin Films: Applications-Led Growth of Functional Materials*, Wiley-Interscience, **2007**.
- [56] I. N. Mihailescu, A. P. Caricato, *Pulsed Laser Ablation: Advances and Applications in Nanoparticles and Nanostructuring Thin Films*, Pan Stanford Publishing Pte. Ltd., **2018**.
- [57] F. Di Fonzo, D. Tonini, A. Li Bassi, C. S. Casari, M. G. Beghi, C. E. Bottani, D. Gastaldi, P. Vena, R. Contro, *Appl. Phys. A Mater. Sci. Process.* **2008**, *93*, 765.
- [58] R. Giannuzzi, M. Balandeh, A. Mezzetti, L. Meda, P. Pattathil, G. Gigli, F. Di Fonzo, M. Manca, *Adv. Opt. Mater.* **2015**, *3*, 1614.
- [59] L. Passoni, F. Ghods, P. Docampo, A. Abrusci, J. Martí-Rujas, M. Ghidelli, G. Divitini, C. Ducati, M. Binda, S. Guarnera, A. Li Bassi, C. S. Casari, H. J. Snaith, A. Petrozza, F. Di Fonzo, *ACS Nano* **2013**, *7*, 10023.
- [60] G. Giuffredi, A. Mezzetti, A. Perego, P. Mazzolini, M. Prato, F. Fumagalli, Y.-C. Lin, C. Liu, I. N. Ivanov, A. Belianinov, M. Colombo, G. Divitini, C. Ducati, G. Duscher, A. A. Puzos, D. B. Geohegan, F. Di Fonzo, *Small* **2020**, *16*, 2004047.
- [61] R. F. Wood, J. N. Leboeuf, K. R. Chen, D. B. Geohegan, A. A. Puzos, *Appl. Surf. Sci.* **1998**, *127–129*, 151.
- [62] R. F. Wood, K. R. Chen, J. N. Leboeuf, A. A. Puzos, D. B. Geohegan, *Phys. Rev. Lett.* **1997**, *79*, 1571.
- [63] M. Mahjouri-Samani, M. Tian, A. A. Puzos, M. Chi, K. Wang, G. Duscher, C. M. Rouleau, G. Eres, M. Yoon, J. Lasseter, K. Xiao, D. B. Geohegan, *Nano Lett.* **2017**, *17*, 4624.
- [64] Y. K. Kim, S. Y. Lee, B. K. Oh, *RSC Adv.* **2016**, *6*, 109978.
- [65] Y. Amao, *J. CO<sub>2</sub> Util.* **2018**, *26*, 623.
- [66] J. E. Pander, D. Ren, Y. Huang, N. W. X. Loo, S. H. L. Hong, B. S. Yeo, *ChemElectroChem* **2018**, *5*, 219.
- [67] Y. Hori, *Mod. Asp. Electrochem.* **2008**, *42*, 89.
- [68] M. Yuan, M. J. Kummer, S. D. Minter, *Chem. A Eur. J.* **2019**, *25*, 14258.
- [69] G. Özgün, N. G. Karagüler, O. Turunen, N. J. Turner, B. I. Binay, *J. Mol. Catal. B* **2015**, *122*, 212.
- [70] T. Ishibashi, M. Higashi, S. Ikeda, Y. Amao, *ChemCatChem* **2019**, *11*, 6227.
- [71] R. K. Yadav, J. Baeg, G. H. Oh, N. Park, K. Kong, J. Kim, D. W. Hwang, S. K. Biswas, *J. Am. Chem. Soc.* **2012**, *134*, 11455.
- [72] R. Barin, D. Biri, S. Rashid-Nadimi, M. A. Asadollahi, *J. CO<sub>2</sub> Util.* **2018**, *28*, 117.
- [73] M. Yuan, S. Sahin, R. Cai, S. Abdellaoui, D. P. Hickey, S. D. Minter, R. D. Milton, *Angew. Chem. Int. Ed.* **2018**, *57*, 6582.
- [74] S. H. Kim, S. Pokhrel, Y. J. Yoo, *J. Mol. Catal. B* **2008**, *55*, 130.

Manuscript received: April 12, 2021  
Revised manuscript received: June 8, 2021